RSC Advances

PAPER

View Article Online
View Journal | View Issue

Cite this: *RSC Adv.*, 2025, **15**, 8784

Near-infrared luminescence from $Li_2ZnGeO_4:Ln^{3+}$ (Ln = Er, Tm, Ho)

Nikola Bednarska-Adam, [a] Marta Kuwik, [a] Tomasz Goryczka,[b] Vitalii Ivanov, [c] Józef Dresner,[d] Wojciech A. Pisarski [a] and Joanna Pisarska *[a]

Received 10th November 2024
Accepted 24th February 2025

DOI: 10.1039/d4ra07999j

rsc.li/rsc-advances

In this work, ceramic compounds $Li_2ZnGeO_4:Ln^{3+}$ (Ln = Er, Tm, Ho), belonging to the family of germanate olivines, were studied. The structural properties were examined using X-ray diffraction, scanning electron microscopy, IR and Raman spectroscopy. Near-infrared luminescence spectra showed that the bands located in the spectral range of 1400–2100 nm were due to the electronic transitions of lanthanide ions: $^4I_{13/2} \rightarrow {}^4I_{15/2}$ (Er^{3+}), $^3H_4 \rightarrow {}^3F_4$ and $^3F_4 \rightarrow {}^3H_6$ (Tm^{3+}), and $^5I_7 \rightarrow {}^5I_8$ (Ho^{3+}). Decay curve analysis indicated that the near-infrared luminescence from the excited states of lanthanide ions in Li_2ZnGeO_4 was relatively long-lived. The results suggest that germanate olivines $Li_2ZnGeO_4:Ln^{3+}$ (Ln = Er, Tm, Ho) are promising inorganic phosphors and can be successfully used as ceramic sources emitting near-infrared radiation.

Introduction

In recent years, near-infrared (NIR) luminescent materials,[1–5] with particular focus on NIR inorganic persistent phosphors,[6,7] have gained significant attention due to their numerous multifunctional applications. Recently published papers report interesting findings regarding the potential applications of NIR persistent phosphors in the third bio-imaging window (NIR-III). Xu and co-workers[8–10] suggested that NIR long persistent luminescence of erbium ions in inorganic phosphors such as garnet $Y_3Al_2Ga_3O_{12}$ or perovskite $LaAlO_3$ can be realized by utilizing efficient energy transfer from Ce^{3+} to Er^{3+} or Cr^{3+} to Er^{3+}, respectively. These inorganic phosphors exhibit long (>10 h) NIR persistent luminescence centered at approximately 1550 nm due to the $^4I_{13/2} \rightarrow {}^4I_{15/2}$ transition of erbium ions, operating in the NIR-III biological window. These aspects are particularly interesting for low-phonon inorganic matrices, especially germanate ceramics, due to their promising optical and dielectric properties.

In general, germanate-based ceramics are very attractive materials for modern visible and near-infrared optoelectronics. Doping with lanthanide ions (Ln^{3+}) enables important multifunctional applications of germanate ceramics, including their use as inorganic phosphors in red-green-blue (RGB) technology. Phosphors of $ABGe_2O_7$ (A = La or Y; B = Al or In) doped with Er^{3+}, Tb^{3+}, Pr^{3+} or Tm^{3+}, emitting red, green or blue light with high color purity, are of interest for displays and lighting devices.[11–14] Eu^{3+}-doped germanate ceramics, such as $Zn_2GeO_4:Eu^{3+}$, $KNaGaGeO_4:Eu^{3+}$, and $Ba_2AGe_2O_7:Eu^{3+}$ (A = Mg or Zn), are thermally stable, efficient red-emitting phosphors, which can be successfully applied to high-resolution and high-sensitivity accurate latent fingerprint detection, multi-mode anti-counterfeiting and white-LED applications.[15–17] Phosphors with the general formula $A_2B_2GeO_7$ (where A = Ca or Sr; B = Al or Ga) doped with Pr^{3+} ions[18,19] and co-doped with Pr^{3+}/Yb^{3+} ions[20] may be applied for c-Si solar cells, biomedical imaging and dynamic multicolor anti-counterfeiting under UV irradiation. The energy transfer processes in germanate ceramics co-doped with Dy^{3+}/Tm^{3+} and Tb^{3+}/Eu^{3+} ions[21,22] have been studied in relation to their practical applications as white-light-emitting diodes. Phosphors, such as Zn_2GeO_4,[23] $Ca_2Al_2Ge_3O_{12}$,[24] and La_4GeO_8,[25] co-doped with Er^{3+}/Yb^{3+} ions have been designed for fingerprint verification, anti-counterfeiting and luminescent thermometry. The influence of Yb^{3+} content on the up-conversion luminescence of Er^{3+} ions in $SrGe_4O_9$ phosphors has also been examined in detail.[26] Further studies revealed that germanate ceramic materials co-doped with transition metal and lanthanide ions are also useful for a wide range of photonic applications, including c-Si solar cells, infrared detectors and long-wavelength NIR LED chips.[27,28]

Among the germanate ceramics, special attention has been paid to compounds with an olivine structure. The $AYGeO_4$ (A = Na or Li) germanate olivines doped with Eu^{3+}, Sm^{3+} or Dy^{3+} have been developed for potential applications in solid-state lighting.[29–31] The variation in the up-conversion luminescence of $LiYGeO_4:Er^{3+}/Yb^{3+}$ phosphors with temperature has been also investigated for optical thermometers and anti-counterfeiting.[32] The results indicate that the modulation of emission color can

[a]*Institute of Chemistry, University of Silesia, 40-007 Katowice, Poland. E-mail: joanna.pisarska@us.edu.pl*
[b]*Institute of Materials Engineering, University of Silesia, 41-500 Chorzów, Poland*
[c]*Institute of Physics, Polish Academy of Sciences, 02-668 Warsaw, Poland*
[d]*Eurotek International, 02-726 Warsaw, Poland*

be realized by changing the laser excitation power, temperature and pumping wavelength. Ceramics with the chemical formula Li_2ZnGeO_4 belong to the same olivine-type germanate family. The energy band gap for Li_2ZnGeO_4 calculated from the Kubelka–Munk equation and Tauc plot method is equal to 5.78 eV.[33] However, the data in the literature indicate that the optical properties of Li_2ZnGeO_4 have been rarely studied. Recently, the published papers mainly focused on the luminescence of Li_2ZnGeO_4 germanate ceramics doped with transition metal ions such as Mn^{2+} and Cr^{4+}. The experimental results suggest that Mn^{2+}-doped Li_2ZnGeO_4 ceramics[34,35] are promising green-emitting phosphors in field-emission displays with high color purity, whereas Cr^{4+}-doped Li_2ZnGeO_4 ceramics are recommended as efficient broadband NIR-II phosphors.[36] Factually, recent work on Ln^{3+}-doped germanate olivines was limited to Li_2ZnGeO_4 with Pr^{3+}, Nd^{3+} or Gd^{3+}, which exhibited enhanced persistent blue luminescence.[37] However, to date, the infrared emission properties of Li_2ZnGeO_4:Ln^{3+} have not been studied. Lastly, the emission properties of $NaYGeO_4$:Tm^{3+} powders in the range of 1300–1600 nm and 1600–2200 nm due to the $^3H_4 \rightarrow {}^3F_4$ and $^3F_4 \rightarrow {}^3H_6$ transitions of Tm^{3+} have been analyzed under 808 nm laser diode excitation.[38] At this moment, it should be also pointed out that Nd^{3+}/Ho^{3+} co-doped $NaLa_9(GeO_4)_6O_2$ phosphors with an apatite structure have been proposed for infrared luminescence applications.[39]

The aim of this work is related to germanate olivines Li_2ZnGeO_4:Ln^{3+} emitting near-infrared radiation in the spectral range of 1400–2100 nm. Lanthanide ions playing an important role as optical dopants were limited to trivalent erbium, thulium and holmium due to their near-infrared luminescence bands located at about 1500 nm (Er^{3+}), 1450/1800 nm (Tm^{3+}) and 2000 nm (Ho^{3+}), respectively. Luminescence bands corresponding to the $^4I_{13/2} \rightarrow {}^4I_{15/2}$ (Er^{3+}), $^3H_4 \rightarrow {}^3F_4$ and $^3F_4 \rightarrow {}^3H_6$ (Tm^{3+}), and $^5I_7 \rightarrow {}^5I_8$ (Ho^{3+}) transitions of Ln^{3+} were analyzed. Our studies showed that the Li_2ZnGeO_4:Ln^{3+} germanate olivines are promising inorganic phosphors and attractive candidate for ceramic sources useful in near-infrared optoelectronics. Our intention was to study the infrared emission properties of Ln^{3+}-doped germanate olivines for the first time. The unique advantages of this study are the characterization of the near-infrared luminescence of Er^{3+}, Tm^{3+} and Ho^{3+} ions in germanate ceramic systems in the range of 1400–2100 nm, which has not been examined and reported before, to the best of our knowledge.

Experimental

$Li_2Zn_{(1-x)}Ln_xGeO_4$:xLn^{3+} (Ln^{3+} = Er^{3+}, Tm^{3+} or Ho^{3+} with a concentration equal to 0.5 mol%) samples in the form of pellets were prepared using the high-purity initial reagents of ZnO (99.99%), GeO_2 (99.99%), and Li_2CO_3 (99.997%), and the appropriate lanthanide oxides of Er_2O_3 (99.999%), Tm_2O_3 (99.999%) or Ho_2O_3 (99.999%) from Sigma-Aldrich Chemical Co. (St. Louis, MO, USA) *via* the conventional high-temperature solid-state reaction method. The appropriate amounts of raw materials were milled and homogenized in an agate mortar for 1 h with C_2H_5OH medium (POCH basic 96% pure). The ground samples were calcined in a non-covered Pt crucible at 1100 °C/6 h in an air atmosphere. The calcination process was divided into two steps, *i.e.*, reaching the temperature of 800 °C/0.5 h, and then 1100 °C/10 min. The calcinated samples were ground again and divided into smaller batches. Pellets with a diameter of 10 mm were formed using a binder (PVA) and cold pressed at 375 MPa. Next, the pellets were subjected to heat treatment to remove the binder at 550 °C/2 h and cooled to room temperature. The samples were sintered at 1200 °C/5 h and cooled to room temperature. The sintering process included several steps of heating to 800 °C/1 h, then sintering for 15 min, heating to 1200 °C and sintering for 5 h.

To characterize the undoped and Ln^{3+}-doped ceramic samples, several measurements were performed, including XRD, SEM, transmittance, Raman and near-infrared emission spectroscopy. The nature of the studied samples was identified using a diffractometer (X'Pert-Pro, PANalytical, Eindhoven, The Netherlands). X-ray diffraction measurements were performed with $CuK_{\alpha 1 \text{ and } 2}$ radiation. The microstructure of the samples was observed using a JSM6480 scanning electron microscope (SEM) along with JSM-7100F TTL LV (Jeol Ltd., Tokyo, Japan). Transmittance spectra were recorded on a Nicolet™ iS™ 50 IR spectrometer. Raman spectra were measured using a Thermo Scientific™ DXR™2xi Raman imaging microscope. Data were recorded with a 455 nm laser (the power 4 mW on samples). Near-infrared luminescence measurements were carried out using a Photon Technology International (PTI) Quanta-Master 40 (QM40) UV/VIS steady-state spectrofluorometer including a double 200 mm monochromator, an Xe lamp (75 W) as the light source, and Hamamatsu H10330B-75 and InGaAs detectors. The spectra were measured with a resolution of ±0.5 nm. For the decay curve measurements, a pulsed tunable optical parametric oscillator (OPO) pumped by the third harmonic of an Nd:YAG laser (Opotek Opolette 355 LD, Carlsband, CA, USA) was used. The decay curves with an accuracy of ±0.5 μs were recorded using a PTI ASOC-10 USB-2500 oscilloscope (Horiba Instruments).

Absolute photoluminescence quantum yield was measured using a Petite integrating sphere (PTI Horiba Instruments), which is the standard accessory for QM40. It replaces the sample holder, and thus no modification of excitation or emission optics was required. The integration sphere had a powder or pellet holder inside it. The method applied used two-step luminescence measurement, with the excitation set to λ_{exc}. Firstly, the entire luminescence spectrum, including the scatter of excitation line around λ_{exc}, was recorded with the "active sample" in the pellet mount. In the second step, the same measurement was executed with the "reference sample", which was prepared in the same way as the active sample, but without Ln^{3+} ions. This procedure guaranteed that all the conditions for sample and reference runs were as similar as possible. Both spectra were actively recorded with real-time emission correction. A QM40 EXCORR real-time excitation source intensity monitor was used to verify the stability of the Xe lamp source. Dark background subtraction before each run was also applied. All measurement conditions were kept identical in both runs with the exception of a neutral density filter to reduce

the intensity of the strong scattered band at λ_{exc} to keep the intensity of this band in the same order as the luminescence band of interest around λ_{em}. Then, the attenuation coefficient was carefully measured. The integral intensities of the scatter $I(\lambda_{exc})$ band and luminescence with any possible trace of the scatter at $I(\lambda_{em})$ for the active and reference samples were calculated and subtracted, respectively, yielding a good representation of the number of photons absorbed and emitted by the sample. The ratio of the latter to the former, corrected by the attenuation factor of the ND filter used resulted in the absolute quantum yield of the $I(\lambda_{em})$ emission band.

Results and discussion

The X-ray diffraction patterns of the undoped Li_2ZnGeO_4 and lanthanide-doped Li_2ZnGeO_4:Ln^{3+} (Ln = Er, Tm, Ho) germanate ceramics are presented in Fig. 1. All the diffraction peaks can be assigned to the Li_2ZnGeO_4 ceramic compounds, which crystallize in a monoclinic lattice with the $P2_1/n$ space group (ICDD PDF-4 database – card no. 00-038-1082). It is also well evident that Ln^{3+} doping had no effect on the crystalline structure and no additional phases related to impurities existed compared to the pure Li_2ZnGeO_4 monoclinic phase. This suggests that Ln^{3+} ions well entered Li_2ZnGeO_4 with an olivine structure.

Further studies using the SEM-BS images (Fig. 2) sensitive to the contrast of the chemical composition confirmed that no other phases, precipitation, or inclusions existed in the undoped and Ln^{3+}-doped ceramic samples. Similar to previously published results for Li_2MgGeO_4 doped with Pr^{3+} and Tm^{3+} ions,[40] the objects shown in the SEM-BS images have an even shade of gray, suggesting that all the ceramic components reacted and only one crystalline phase of Li_2ZnGeO_4 was formed.

Previous investigations on Li_2ZnGeO_4 ceramics using Raman spectroscopy revealed that bands observed in the low frequency range below 400 cm^{-1} correspond to the wagging and twisting vibrations of the GeO_4 tetrahedra.[41,42] Fig. 3 shows the Raman spectrum measured in the higher frequency region, which

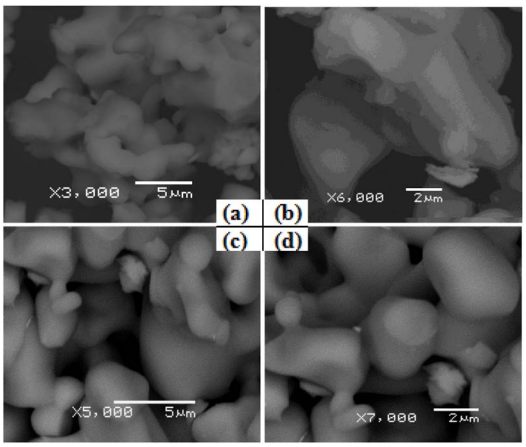

Fig. 2 Ceramic particles observed with SEM-BE images: (a) undoped sample and samples doped with (b) Er^{3+}, (c) Tm^{3+} and (d) Ho^{3+} ions.

consists of two groups of bands. These two groups are located in the frequency range of 440–550 cm^{-1} and 650–850 cm^{-1}, respectively. The first group of bands near 442 cm^{-1}, 494 cm^{-1} and 529 cm^{-1} is related to the bending vibrations of the GeO_4 groups.[33] In the second group, the three bands located at about 725 cm^{-1}, 752 cm^{-1} and 820 cm^{-1} are due to the stretching vibrations of the GeO_4 groups.[43] Based on previous results obtained for zinc germanate nanomaterials, Zn_2GeO_4, the Raman bands located at 750 cm^{-1} and 820 cm^{-1} were assigned to the symmetric and asymmetric stretching vibration of the Ge–O–Zn bond, respectively.[44]

Numerous near-infrared luminescent materials containing lanthanide and/or transition metal ions have been reported.[1] Among them, low-phonon germanate ceramics seem to be perspective emerging infrared luminescent materials for next-generation optoelectronic devices.[45] In particular, there has been a significant increase in the search for germanate-based materials emitting infrared radiation in the spectral range of 1400–2100 nm.[46,47] Near-infrared laser sources are an attractive scientific topic due to their various fields of applications such as

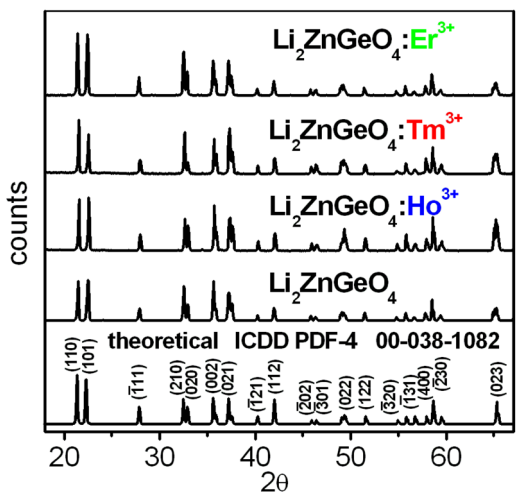

Fig. 1 X-ray diffraction patterns of Li_2ZnGeO_4 and Li_2ZnGeO_4:Ln^{3+}.

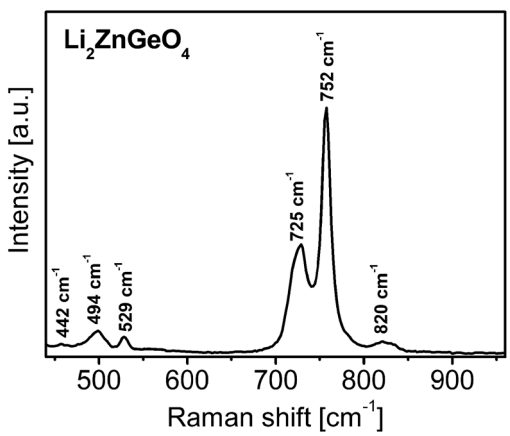

Fig. 3 Raman spectrum of germanate ceramics Li_2ZnGeO_4.

laser remote chemical sensing, medical surgery and atmospheric monitoring. They can be also applied as the main components in eye-safe laser radars and optical amplifiers. In this spectral region, materials doped with Er^{3+}, Tm^{3+} and Ho^{3+} can emit infrared radiation due to their characteristic intra-configurational 4f–4f electronic transitions. Based on absorption and luminescence spectra measurements, the energy level diagram including main laser transitions at 1450 nm, 1550 nm 1800 nm and 2000 nm was constructed for numerous germanate-based compounds doped with Er^{3+}, Tm^{3+} and Ho^{3+}, which have been studied systematically by us in detail.[48–54] The near-infrared luminescence bands of the Ln^{3+} ions correspond to the $^4I_{13/2} \rightarrow {}^4I_{15/2}$ (Er^{3+}) transition located at 1550 nm, the $^3H_4 \rightarrow {}^3F_4$ and $^3F_4 \rightarrow {}^3H_6$ (Tm^{3+}) transitions near 1450 nm and 1800 nm, and the $^5I_7 \rightarrow {}^5I_8$ (Ho^{3+}) transition at 2000 nm. They are schematically illustrated in the energy level diagram of Ln^{3+} ions shown in Fig. 4.

According to transmittance spectrum measurements, it is well known that the infrared band located near 3400 cm^{-1} is due to the stretching vibrations of hydroxyl groups. The relatively high content of hydroxyl groups effectively quenches the emission from the excited states of Ln^{3+} ions in different compounds. This phenomenon is especially important for Er^{3+},[55–57] Tm^{3+},[58] and Ho^{3+} ions[59] in inorganic glasses emitting near-infrared radiation at 1550 nm (6450 cm^{-1}), 1800 nm (5550 cm^{-1}) and 2000 nm (5000 cm^{-1}) because less than two vibrations of OH^- groups can effectively bridge the energy gaps between $^4I_{13/2}$ and $^4I_{15/2}$ (Er^{3+}), $^3F_4$ and $^3H_6$ (Tm^{3+}), and $^5I_7$ and $^5I_8$ (Ho^{3+}), and quench the near-infrared emission. Structural transformation from glasses (completely amorphous) to glass–ceramic materials (partially crystallized) progressively results in a decrease in the number of hydroxyl groups with an increase in heat-treatment temperature.[60] Further systematic studies suggest that the increase in the photoluminescence intensity of the lanthanide ions with the calcination temperature is attributed to the removal of the hydroxyl groups.[61] Thus, the high-temperature sintering process (1200 °C/5 h) used for the preparation of the Li_2ZnGeO_4:Ln^{3+} germanate ceramics, where Ln denotes Er, Tm or Ho (see Experimental section), can efficiently reduce the OH^- content. The results from the transmittance spectrum measurements given in Fig. 5 show that the IR band intensity near 3400 cm^{-1} is extremely low and nearly invisible compared to our previous results for oxide and oxyfluoride germanate glass systems based on $BaO–Ga_2O_3–GeO_2$ (BGG), where the IR absorption coefficients, α_{OH}, are close to 0.25 cm^{-1} (0% BaF_2) and 0.020 cm^{-1} (10% BaF_2), respectively.[50] This suggests that the presence of OH^- groups cannot make a substantial contribution to the luminescence quenching from the excited states of Ln^{3+} ions (Ln = Er, Tm, Ho) in the Li_2ZnGeO_4 germanate olivines.

Initially, the near-infrared emission spectra and decays of Li_2ZnGeO_4:Ln^{3+} (Ln = Er, Tm, Ho) were tested under different excitation wavelengths. The spectra measured for the Ln^{3+}-doped samples show near-infrared luminescent bands corresponding to the characteristic electronic transitions of Ln^{3+} ions at 1550 nm (Ln = Er), 1450 nm and 1800 nm (Ln = Tm) and 2000 nm (Ln = Ho), as schematized in the energy level diagram (Fig. 4). These optical effects were not observed for the undoped Li_2ZnGeO_4 sample, which is experimental proof for the presence of lanthanide ions (Er^{3+}, Tm^{3+} or Ho^{3+}) in the final products. Generally, it is also accepted for inorganic phosphors that each excited state of Ln^{3+} ions further splits under the influence of the crystal field produced by the chemical environment.[62] Thus, the broad emission bands consist of several Stark components induced by the crystal field and their spectral profiles are usually unsymmetrical. The comparative studies indicated that the infrared emission peaks originating from sub-levels of erbium ions are quite well-resolved and the Stark level structures of multiplets depending on the crystalline field of the inorganic matrices are completely different for the Y_2O_3:Er^{3+}, Sc_2O_3:Er^{3+} and YF_3:Er^{3+} systems.[63] In the case of

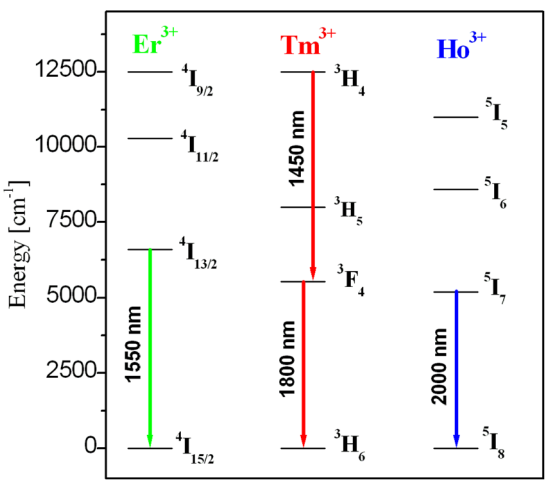

Fig. 4 Energy level diagram of Ln^{3+} ions, with near-infrared luminescence transitions indicated.

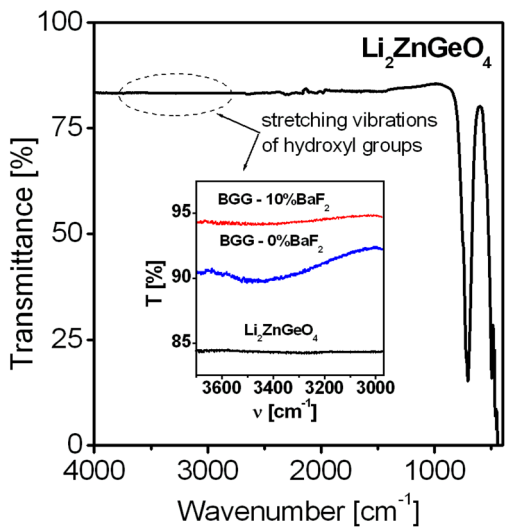

Fig. 5 Transmittance spectrum of germanate ceramics Li_2ZnGeO_4. Inset shows the transmittance bands due to the stretching vibration of OH^- groups. For comparison, the results for germanate glass (BGG) are also given.

Li_2ZnGeO_4:Ln^{3+} (where Ln denotes Er, Tm or Ho), its Stark level structure of multiplets is rather less evidenced and the experimental results are comparable to the $NaLaMgWO_6$ inorganic phosphors emitting near-infrared radiation from sub-levels of Nd^{3+} and Er^{3+} ions.[64]

The preliminary spectroscopic results for the Er^{3+}, Tm^{3+} and Ho^{3+} ions in the Li_2ZnGeO_4 olivines indicate that the profiles of the emission bands and decays from the excited states of Ln^{3+} are nearly independent of the excitation wavelength. This suggests that the Ln^{3+} ions occupy only one site in Li_2ZnGeO_4, in contrast to Y_2SiO_5 (ref. 65) or $CaSc_2O_4$,[66,67] where two Er^{3+} centers were identified using emission spectroscopy. At this moment, it should be noticed that the atomic positions of Zn^{2+} may be occupied by Ln^{3+}. This was observed earlier for similar germanate olivines, Li_2SrGeO_4:RE^{3+}, where the positions of the divalent Sr^{2+} were occupied by trivalent lanthanide (Ce^{3+}, Tb^{3+}, or Dy^{3+}) ions.[68]

Fig. 6 presents the near-infrared luminescence spectrum of Li_2ZnGeO_4:Er^{3+} excited at 980 nm line. The characteristic emission band at 1542 nm corresponds to the $^4I_{13/2} \rightarrow {}^4I_{15/2}$ (Er^{3+}) transition. The excitation spectrum for Li_2ZnGeO_4:Er^{3+} measured by monitoring the emission wavelength at 1542 nm is presented in the inset of Fig. 6. The band located at 980 nm corresponds to the transition originating from the $^4I_{15/2}$ ground state to the $^4I_{11/2}$ excited state of Er^{3+}.

Fig. 7 shows the emission decay from the $^4I_{13/2}$ state of Er^{3+}. Previous studies demonstrated that the emission decays from the $^4I_{13/2}$ state of Er^{3+} in some ceramic compounds can vary greatly with experimental values ranging from microseconds to milliseconds. In fact, the $^4I_{13/2}$ lifetime of Er^{3+} ions changed from 370 μs for Ca_2SiO_4:Er^{3+} phosphors obtained from agro-food waste materials[69] to 9.5 ms for Ba(Zr, Mg, Ta)O_3:Er^{3+} perovskite ceramics.[70] In our case, the decay curve was well fitted using a mono-exponential function given by $I(t) = I_0 \exp(t/\tau_m)$ and the calculated luminescence lifetime $^4I_{13/2}$ (Er^{3+}) in the

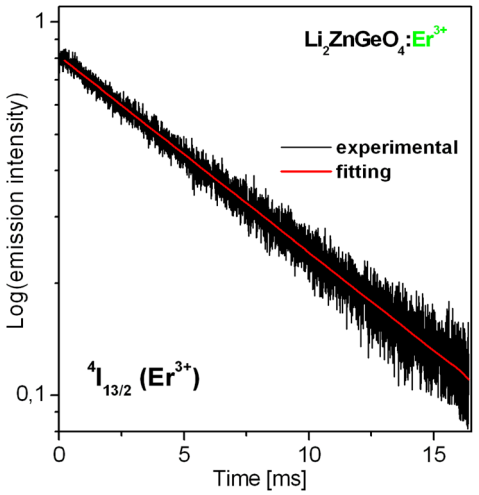

Fig. 7 Luminescence decay from the $^4I_{13/2}$ excited state of Er^{3+} ions.

Li_2ZnGeO_4 germanate ceramics possessing an olivine structure is nearly 8.27 ms. The Li_2ZnGeO_4:Er^{3+} germanate ceramics exhibit a relatively large $^4I_{13/2}$ lifetime compared to the values obtained for similar oxide phosphors documented in the literature. For example, the luminescence decay from the $^4I_{13/2}$ state is considerably longer compared with the values for Er^{3+} ions in ZnO semiconductor quantum dots[71] and germanate compounds.[72–74]

Fig. 8 presents the near-infrared luminescence spectrum of the Li_2ZnGeO_4:Tm^{3+} germanate olivines under 797 nm excitation. The inset shows the excitation spectrum measured on monitoring the emission wavelength at 1802 nm, where the two characteristic bands are related to the $^3F_2$,$^3F_3 \rightarrow {}^3H_6$ (650–700 nm) and $^3H_4 \rightarrow {}^3H_6$ (797 nm) transitions of the Tm^{3+} ions. The latter transition near 800 nm, *i.e.* $^3H_4 \rightarrow {}^3H_6$ transition, is often

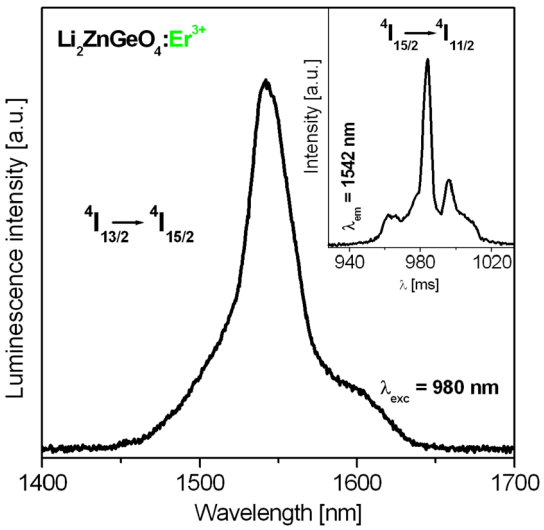

Fig. 6 Near-infrared emission spectrum of Li_2ZnGeO_4:Er^{3+}. The inset shows the excitation spectrum under monitoring the emission wavelength at 1542 nm.

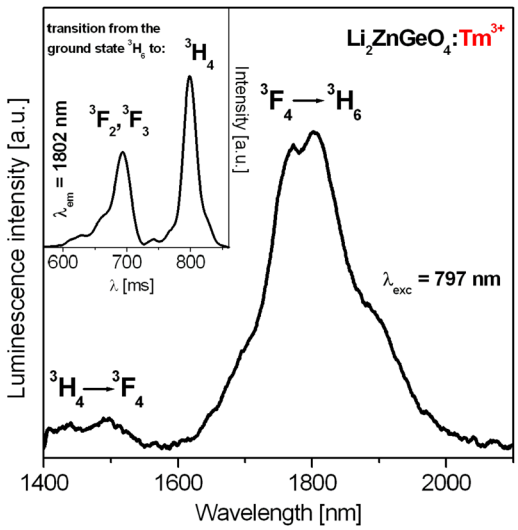

Fig. 8 Near-infrared emission spectrum of Li_2ZnGeO_4:Tm^{3+}. The inset shows the excitation spectrum under monitoring the emission wavelength at 1802 nm.

used as the excitation line to examine the up-conversion processes and near-infrared luminescence properties of thulium ions in numerous inorganic compounds.[75,76]

Two emission bands were observed for Tm^{3+} in the studied spectral range of 1400–2100 nm under 797 nm excitation. The near-infrared emission bands correspond to the $^3H_4 \rightarrow {}^3F_4$ and $^3F_4 \rightarrow {}^3H_6$ transitions of Tm^{3+}. The near-infrared luminescence band near 1450 nm corresponding to the $^3H_4 \rightarrow {}^3F_4$ transition of the Tm^{3+} ions was successfully quenched due to the presence of a cross-relaxation (CR) process between the $^3H_4$ excited state and $^3H_6$ ground state. The $^3H_4$ state is quickly depopulated because the cross-relaxation process between pairs of Tm^{3+}: $^3H_4 + {}^3H_6 \rightarrow {}^3F_4 + {}^3F_4$ is very efficient.[77–81] Consequently, the intensity of the near-infrared emission band centered at 1802 nm due to the $^3F_4 \rightarrow {}^3H_6$ transition is significantly strong. Moreover, the emission linewidth for the $^3F_4 \rightarrow {}^3H_6$ transition of thulium in Li_2ZnGeO_4:Tm^{3+} defined as the full width at half maximum (FWHM) is relatively broad and equals 145 nm.

Fig. 9 shows the emission decays from the $^3H_4$ and $^3F_4$ states of thulium ions in the olivine Li_2ZnGeO_4:Tm^{3+}. In both cases, the emission decay curves become nearly mono-exponential. Based on the decays, the luminescence lifetimes for both the $^3H_4$ and $^3F_4$ excited states of Tm^{3+} ions were determined. The values of the emission lifetimes are close to 0.2 ms ($^3H_4$) and 2.14 ms ($^3F_4$), respectively. This indicates that the lifetime of Tm^{3+} (0.5 mol%) is nearly 10-fold larger for the $^3F_4$ state than the $^3H_4$ state. Interestingly, similar effects were also observed for Tm^{3+} ions in apatite-type germanate phosphors with the chemical formula $NaLa_9(GeO_4)_6O_2$, where the activator concentration-dependent decay times were larger for the $^3F_4$ state (133–1313 μs) than the $^3H_4$ state (19–432 μs).[82]

Finally, the germanate ceramics with an olivine structure doped with Ho^{3+} ions were investigated. In general, Ho^{3+}-doped germanates belonging to the family of low-phonon systems are known as efficient compounds emitting near-infrared radiation at 2000 nm.[53] However, the infrared emission properties of Ho^{3+} ions in germanate ceramics have not been studied to date, to the best of our knowledge. Recently, Ho^{3+}:Y_2O_3–MgO nanocomposite ceramics have been proposed as new promising IR emitting materials for use in high-power eye-safe laser systems operating in the 2 μm wavelength range.[83] Previous works published by Singh *et al.*[84–86] focused on green light emitting phosphors containing Ho^{3+}. Here, the results for Li_2ZnGeO_4:Ho^{3+} emitting IR radiation near 2000 nm are presented and discussed. The near-infrared emission spectrum corresponding to the $^5I_7 \rightarrow {}^5I_8$ transition of Ho^{3+} ions is presented in Fig. 10.

The emission spectrum centered at 1998 nm was measured under 450 nm excitation. The value of FWHM for the $^5I_7 \rightarrow {}^5I_8$ transition of Ho^{3+} is equal to 112 nm. The inset presents the excitation spectrum for Li_2ZnGeO_4:Ho^{3+} measured by monitoring the emission wavelength at 1998 nm. The spectrum consists of bands assigned to transitions of Ho^{3+} ions, which originate from the $^5I_8$ ground state to the higher-lying $^5G_{4,5}$, $^5G_6$, $^5F_{2,3}$ and $^5S_2$, $^5F_4$ excites states. The intensity of band centered at 450 nm due to the $^5I_8 \rightarrow {}^5G_6$ transition is considerably higher compared to other bands. Therefore, the 450 nm excitation line is often chosen to measure the near-infrared emission properties of holmium ions.[87] Fig. 11 shows the nearly mono-exponential luminescence decay from the $^5I_7$ state of holmium ions in the Li_2ZnGeO_4:Ho^{3+} germanate olivine.

Based on the decay measured from the $^5I_7$ state of holmium in Li_2ZnGeO_4:Ho^{3+}, the emission lifetime was calculated and its experimental value is close to 6.98 ms. The lifetime $^5I_7$ (Ho^{3+}) in the Li_2ZnGeO_4:Ho^{3+} germanate olivine is comparable with the values obtained for $Y_3Al_5O_{12}$:Ho^{3+} ceramics (τ = 7.04 ms) produced from laser-ablated nanoparticles[88] and $Yb_3Ga_5O_{12}$ nanocrystals with 0.5% Ho^{3+} (τ = 7.77 ms) synthesized *via* the sol–gel combustion technique using citric acid.[89]

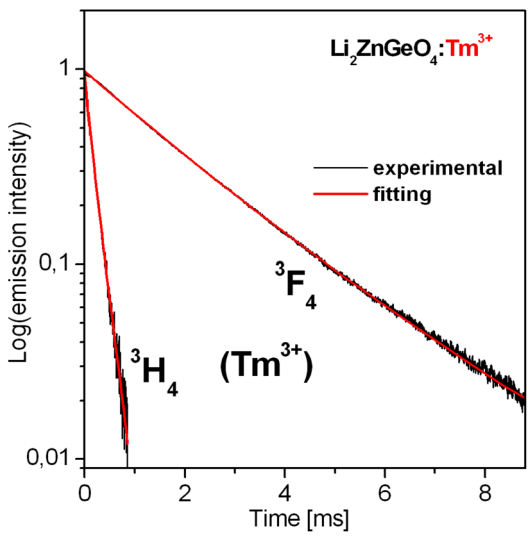

Fig. 9 Luminescence decays from the $^3H_4$ and $^3F_4$ excited states of Tm^{3+}.

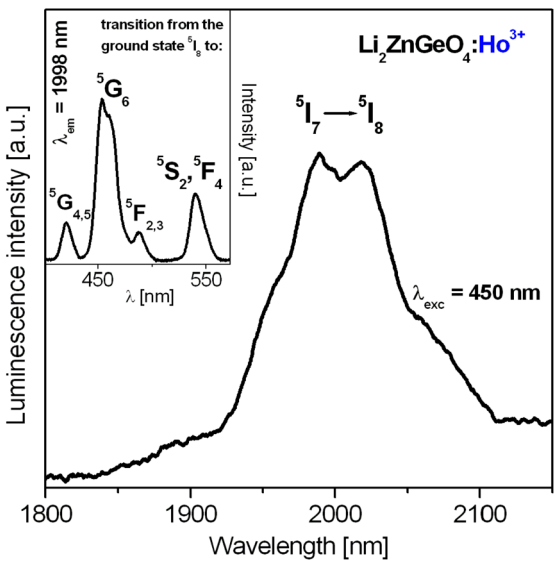

Fig. 10 Near-infrared emission spectrum of Li_2ZnGeO_4:Ho^{3+}. The inset shows the excitation spectrum under monitoring the emission wavelength at 1998 nm.

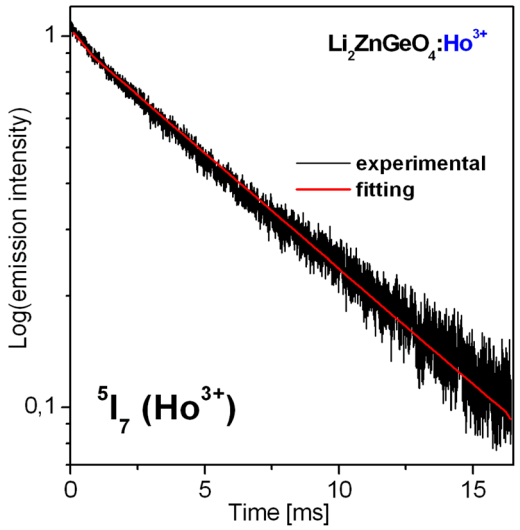

Fig. 11 Luminescence decay from the $^5I_7$ excited state of Ho^{3+} ions.

Finally, the photoluminescence quantum yield (PLQY), which is defined as the ratio of the number of emitted photons to the number of absorbed photons, was determined by the absolute method using an integrating sphere.[90] Among the infrared phosphors, the determination of the absolute photoluminescence quantum yield is mainly limited to erbium-doped compounds emitting radiation near 1500 nm under 980 excitation. For example, literature data indicates that the PLQY values changed significantly from 3.6% (in water) for poly(-acrylic acid) (PAA)-modified $NaLnF_4$:40Gd/20Yb/2Er nanorods[91] up to even 18.7% for $NaErF_4$@$NaYbF_4$@$NaYF_4$ nanoparticles,[92] 32.8% for $NaCeF_4$:Er/Yb nanocrystals,[93] and 35.74% for Ce^{3+}/Er^{3+}:$LiYbF_4$ nanocrystals.[94] Further luminescent studies on up-converted PbF_2:Er^{3+}/Yb^{3+} crystals fabricated using the Bridgman method well demonstrated that the PLQY values varied from 2.7% to 4.5%, depending on the activator (Er^{3+}/Yb^{3+}) content.[95] In our case, the absolute quantum yield of NIR luminescence near 1550 nm (excited at 988 nm) for the Li_2ZnGeO_4:Er^{3+} sample in the powder pellet form is close to 5.9% and its value is comparable to the experimental results (PLQY = 6%) obtained for core–shell nanostructures with homogeneous core (α-$NaYF_4$:Yb^{3+}/Er^{3+}) and shell (α-$NaYF_4$) domains.[96] However, the latter PLQY value increased to 30% in the case of α-$NaYF_4$:Yb^{3+}/Er^{3+} core–shell structures with heterogeneous (CaF_2) shell domains. A similar situation was observed for the same α-$NaYF_4$:Yb^{3+}/Er^{3+} core–shell systems with Ce^{3+} co-doping. The structural transformation from homogeneous (α-$NaYF_4$) to heterogeneous (CaF_2) shell domains strongly influenced the PLQY values determined for α-$NaYF_4$:Yb^{3+}/Er^{3+}/Ce^{3+} core nanocrystals. Thus, the absolute quantum yield increased drastically from 24% up to 50% at 60 mW cm^{-2}; one of the highest reported PLQY values to date.[96]

In summary, we can conclude that the near-infrared luminescence of lanthanides (Er^{3+}, Tm^{3+}, Ho^{3+}) in the studied Li_2ZnGeO_4 olivines is quite long-lived. Our experimental studies based on near-infrared luminescence spectra and their decays indicate that the Li_2ZnGeO_4:Ln^{3+} (Ln = Er, Tm, Ho) germanate olivines are promising inorganic phosphors and can be successfully used as ceramic sources emitting near-infrared radiation.

Conclusion

The near-infrared luminescence properties of Li_2ZnGeO_4:Ln^{3+} (Ln = Er, Tm, Ho) ceramic phosphors belonging to the family of germanate olivines were investigated for the first time. Their spectra showed near-infrared emission bands centered at 1550 nm, 1450 nm, 1800 nm and 2000 nm, corresponding to $^4I_{13/2} \rightarrow {}^4I_{15/2}$ (Er^{3+}), $^3H_4 \rightarrow {}^3F_4$ and $^3F_4 \rightarrow {}^3H_6$ (Tm^{3+}), as well as $^5I_7 \rightarrow {}^5I_8$ (Ho^{3+}) transitions, respectively. The decay curve analysis demonstrated that the lifetimes for the excited states of Ln^{3+} (Ln = Er, Tm, Ho) are relatively long. The experimental results showed that the Li_2ZnGeO_4:Ln^{3+} germanate olivines are attractive inorganic phosphors and can be applied as ceramic sources emitting near-infrared radiation.

Data availability

The data are available upon request from the authors.

Author contributions

Conceptualization, project administration, resources and funding acquisition: Joanna Pisarska. Investigation and validation: Nikola Bednarska-Adam prepared the ceramic samples. Nikola Bednarska-Adam and Marta Kuwik performed spectroscopic and optical experiments. Tomasz Goryczka performed the XRD and SEM experiments. Vitalii Ivanov and Józef Dresner performed the absolute photoluminescence quantum yield test. Methodology: Joanna Pisarska and Wojciech A. Pisarski. Formal analysis and supervision: Wojciech A. Pisarski. Writing – original draft: Joanna Pisarska. Writing – review & editing: Joanna Pisarska.

Conflicts of interest

There are no conflicts to declare.

Acknowledgements

The National Science Centre (Poland) supported this work under project no. 2019/35/B/ST5/01924. The publication was co-financed by the funds granted under the Research Excellence Initiative of the University of Silesia in Katowice.

References

1 H.-H. Li, Y.-K. Wang and L.-S. Liao, Near-Infrared Luminescent Materials Incorporating Rare Earth/Transition Metal Ions: From Materials to Applications, *Adv. Mater.*, 2024, **36**, 2403076, DOI: 10.1002/adma.202403076.
2 G. Zheng, C. Lou, Z. Yuan, W. Xiao, L. Shang, J. Zhong, M. Tang and J. Qiu, Rare-Metal-Free Ultrabroadband Near-

Infrared Phosphors, *Adv. Mater.*, 2025, **37**, 2415791, DOI: 10.1002/adma.202415791.

3 G. N. A. De Guzman, S.-F. Hu and R.-S. Liu, Enticing applications of near-infrared phosphors: review and future perspectives, *J. Chin. Chem. Soc.*, 2021, **68**, 206–215, DOI: 10.1002/jccs.202000287.

4 G. N. A. De Guzman, M.-H. Fang, C.-H. Liang, Z. Bao, S.-F. Hu and R.-S. Liu, Near-infrared phosphors and their full potential: a review on practical applications and future perspectives, *J. Lumin.*, 2020, **219**, 116944, DOI: 10.1016/j.jlumin.2019.116944.

5 V. Rajendran, H. Chang and R.-S. Liu, Recent progress on broadband near-infrared phosphors-converted light emitting diodes for future miniature spectrometers, *Opt. Mater.: X*, 2019, **1**, 100011, DOI: 10.1016/j.omx.2019.100011.

6 J. Xu, M. Back and S. Tanabe, Near-infrared phosphors with persistent luminescence over 1000 nm for optical imaging, in *Phosphor Handbook: Experimental Methods for Phosphor Evaluation and Characterization*, ed. R.-S. Liu and X.-J. Wang, CRS Press, 3rd edn, 2022, ch. 11, pp. 363–418, DOI: 10.1201/9781003098669.

7 Z. Zhou, Y. Li and M. Peng, Near-infrared persistent phosphors: synthesis, design, and applications, *Chem. Eng. J.*, 2020, **399**, 125688, DOI: 10.1016/j.cej.2020.125688.

8 J. Xu, D. Murata, J. Ueda, B. Viana and S. Tanabe, Toward Rechargeable Persistent Luminescence for the First and Third Biological Windows *via* Persistent Energy Transfer and Electron Trap Redistribution, *Inorg. Chem.*, 2018, **57**, 5194–5203, DOI: 10.1021/acs.inorgchem.8b00218.

9 J. Xu, D. Murata, Y. Katayama, J. Ueda and S. Tanabe, Cr^{3+}/Er^{3+} co-doped $LaAlO_3$ perovskite phosphor: a near-infrared persistent luminescence probe covering the first and third biological windows, *J. Mater. Chem. B*, 2017, **5**, 6385–6393, DOI: 10.1039/C7TB01332A.

10 J. Xu, D. Murata, J. Ueda and S. Tanabe, Near-infrared long persistent luminescence of Er^{3+} in garnet for the third bio-imaging window, *J. Mater. Chem. C*, 2016, **4**, 11096–11103, DOI: 10.1039/c6tc04027f.

11 Y.-C. Li, Y.-H. Chang, Y.-F. Lin, Y.-J. Lin and Y.-S. Chang, High color purity phosphors of $LaAlGe_2O_7$ doped with Tm^{3+} and Er^{3+}, *Appl. Phys. Lett.*, 2006, **89**, 081110, DOI: 10.1063/1.2337275.

12 H.-J. Lin and Y.-S. Chang, Blue-Emitting Phosphor of $YInGe_2O_7$ Doped with Tm^{3+} Ions, *Electrochem. Solid-State Lett.*, 2007, **10**, J79–J82, DOI: 10.1149/1.2732076.

13 Y.-S. Chang, H.-J. Lin, Y.-C. Li, Y.-L. Chai and Y.-Y. Tsai, Synthesis and luminescent properties of Tb^{3+}-activated yttrium indium germanate phosphor, *J. Solid State Chem.*, 2007, **180**, 3076–3081, DOI: 10.1016/j.jssc.2007.07.018.

14 L.-G. Teoh, M.-T. Tsai, Y.-C. Chang and Y.-S. Chang, Photoluminescence properties of Pr^{3+} ion-doped $YInGe_2O_7$ phosphor under an ultraviolet irradiation, *Ceram. Int.*, 2018, **44**, 2656–2660, DOI: 10.1016/j.ceramint.2017.10.163.

15 X. Chen, X. Sha, Y. Zhang, D. Gao, L. Wang, Y. Zhang, X. Zhang, J. Zhang, Y. Cao, Y. Wang, X. Li, S. Xu, H. Yu and B. Chen, Eu^{3+} doped zinc germanate long persistent luminescence phosphor for multi-mode anti-counterfeiting application, *J. Lumin.*, 2024, **274**, 120724, DOI: 10.1016/j.jlumin.2024.120724.

16 Q. Zhao, J. Chen, X. Jing, T. Lang, M. Cai, L. Peng, Q. Qiang, W. Chen, E. F. Polisadova and B. Liu, A novel highly efficient Eu^{3+} doped germanate red phosphor for accurate latent fingerprint detection and WLED applications, *J. Lumin.*, 2024, **276**, 120878, DOI: 10.1016/j.jlumin.2024.120878.

17 C. Jia, T.-H. Huang, Z. Huang, J. Wen, W. Xie, X. Tian, T. Wu, H. He and Y. Peng, High thermal stability and colour saturation red-emitting $Ba_2AGe_2O_7$:Eu^{3+} (A = Mg, Zn) phosphors for WLEDs, *J. Lumin.*, 2019, **216**, 116734, DOI: 10.1016/j.jlumin.2019.116734.

18 L. Ji, J. Zhou, J. Zhang, Z. Zhang, Z. Ma, W. Wang, H. Li and C. Wu, A multicolor persistent luminescent phosphor $Sr_2Ga_2GeO_7$:Pr^{3+} for dynamic anticounterfeiting, *J. Am. Ceram. Soc.*, 2019, **102**, 5465–5470, DOI: 10.1111/jace.16432.

19 T. Shen, S. Zhao, A. Su, H. Liu, F. Chen, B. Li, X. Han, D. Yu and D. Zhang, Visible/near-infrared luminescence and concentration effects of Pr^{3+}-doped $Sr_2Al_2GeO_7$ downconversion phosphors, *APL Mater.*, 2024, **12**, 091103, DOI: 10.1063/5.0226329.

20 Z. Zou, L. Feng, C. Cao, J. Zhang and Y. Wang, Near-infrared quantum cutting long persistent luminescence, *Sci. Rep.*, 2016, **6**, 24884, DOI: 10.1038/srep24884.

21 Y. Cao, X. Ding and Y. Wang, A Single-Phase Phosphor $NaLa_9(GeO_4)_6O_2$:Tm^{3+},Dy^{3+} for Near Ultraviolet-White LED and Field-Emission Display, *J. Am. Ceram. Soc.*, 2016, **99**, 3696–3704, DOI: 10.1111/jace.14394.

22 X. Chen, H. Zhang, Z. Liu, J. Qiu and X. Xu, High quality germanate phosphor $La_{(2-x-y)}Ge_2O_7$:Tb^{3+},Eu^{3+} for WLED applications, *J. Lumin.*, 2022, **252**, 119295, DOI: 10.1016/j.jlumin.2022.119295.

23 X. Chen, X. Sha, Y. Zhang, D. Gao, L. Wang, Y. Zhang, T. Liu, X. Zhang, J. Zhang, Y. Cao, Y. Wang, X. Li, S. Xu, H. Yu and B. Chen, Multicolor-emitting Er^{3+} and Er^{3+}/Yb^{3+} doped Zn_2GeO_4 phosphors combining static and dynamic identifications for advanced anti-counterfeiting application, *Spectrochim. Acta, Part A*, 2024, **309**, 123830, DOI: 10.1016/j.saa.2023.123830.

24 J. Zhang, Z. Wang, P. Liu, X. Huo, Y. Wang, H. Suo, L. Li and P. Li, Dual-mode luminous and afterglow $Ca_2Al_2Ge_3O_{12}$:Yb^{3+},Er^{3+} phosphors for anti-counterfeiting and fingerprint verification, *Ceram. Int.*, 2024, **50**, 2436–2442, DOI: 10.1016/j.ceramint.2023.11.029.

25 S. J. Xu, Y. H. Chen, Y. Jiang, G. A. Ashraf and H. Guo, Up-conversion La_4GeO_8:Er^{3+},Yb^{3+} optical thermometer based on fluorescence intensity ratio technique, *J. Lumin.*, 2022, **251**, 119193, DOI: 10.1016/j.jlumin.2022.119193.

26 D. Chavez, C. R. Garcia, J. Oliva, E. Montes, A. I. Mtz-Enriquez, M. A. Garcia-Lobato and L. A. Diaz-Torres, Effect of Yb^{3+} concentration on the green-yellow upconversion emission of $SrGe_4O_9$:Er^{3+} phosphors, *Ceram. Int.*, 2019, **45**, 16911–16917, DOI: 10.1016/j.ceramint.2019.05.236.

27 W. Yang, S. Xiao, X. Yang and Y. Zhao, Broad-band sensitized visible up-conversion in $Y_2Mg_3Ge_3O_{12}$:Ni^{2+},Er^{3+},Nb^{5+} phosphors, *Mater. Adv.*, 2022, **3**, 6050, DOI: 10.1039/d2ma00519k.

28 S. He, Y. Liu, T. Gao, R. Liu, G. Chen, M. Duan and M. Cao, Enhanced luminescence of long-wavelength broadband near-infrared germanate phosphors, *ACS Omega*, 2023, **8**, 15698–15707, DOI: 10.1021/acsomega.3c00995.

29 J. Zhang, B. Liu, Y. Dai and B. Han, Synthesis and luminescence properties of novel host-sensitized germanate phosphors $NaYGeO_4$:Ln (Ln=Eu^{3+}, Sm^{3+}, Dy^{3+}), *Optik*, 2020, **203**, 163944, DOI: 10.1016/j.ijleo.2019.163944.

30 B. Han, Y. Chen, B. Liu and J. Zhang, Solid state synthesis and luminescence properties of Eu^{3+} doped $NaYGeO_4$ phosphors, *Optik*, 2021, **242**, 167177, DOI: 10.1016/j.ijleo.2021.167177.

31 T. Dai, G. Ju, Y. Lv, Y. Jin, H. Wu and Y. Hu, Luminescence properties of novel dual-emission (UV/red) long afterglow phosphor $LiYGeO_4$:Eu^{3+}, *J. Lumin.*, 2021, **237**, 118193, DOI: 10.1016/j.jlumin.2021.118193.

32 H. Cui, Y. Cao, Y. Zhang, L. Li, G. Li, S. Xu, Y. Wang, J. Zhang and B. Chen, Upconversion luminescence thermal enhancement and emission color modulation of $LiYGeO_4$:Er^{3+}/Yb^{3+} phosphors, *J. Alloys Compd.*, 2022, **927**, 167107, DOI: 10.1016/j.jallcom.2022.167107.

33 N. Bednarska-Adam, M. Kuwik, T. Goryczka, B. Macalik, W. A. Pisarski and J. Pisarska, Down- and up-conversion luminescence processes in olivine-type ceramic phosphors Li_2AGeO_4:Er^{3+} (A = Zn, Mg), *Opt. Mater.*, 2023, **143**, 114301, DOI: 10.1016/j.optmat.2023.114301.

34 M. Shang, G. Li, D. Yang, X. Kang, C. Peng and J. Lin, Luminescence properties of Mn^{2+}-doped Li_2ZnGeO_4 as an efficient green phosphor for field-emission displays with high color purity, *Dalton Trans.*, 2012, **41**, 8861–8868, DOI: 10.1039/c2dt30670k.

35 Y. Jin, Y. Hu, H. Duan, L. Chen and X. Wang, The long persistent luminescence properties of phosphors: Li_2ZnGeO_4 and Li_2ZnGeO_4:Mn^{2+}, *RSC Adv.*, 2014, **4**, 11360–11366, DOI: 10.1039/c3ra47760f.

36 S. Yuan, Z. Mu, L. Lou, S. Zhao, D. Zhu and F. Wu, Broadband NIR-II phosphors with Cr^{4+} single activated centers based on special crystal structure for nondestructive analysis, *Ceram. Int.*, 2022, **48**, 26884–26893, DOI: 10.1016/j.ceramint.2022.05.391.

37 T. Tu and G. Jiang, Enhanced persistent luminescence of Li_2ZnGeO_4 host by rare-earth ions (Pr^{3+}, Nd^{3+} and Gd^{3+}) doping, *J. Mater. Sci.: Mater. Electron.*, 2018, **29**, 3146–3152, DOI: 10.1007/s10854-017-8247-x.

38 A. A. Melentsova, O. A. Lipina, M. A. Melkozerova, A. N. Enyashin, A. Y. Chufarov, A. P. Tyutyunnik and V. G. Zubkov, Infrared luminescence properties and energy transfer mechanism in $NaYGeO_4$:Tm^{3+} powders, *Ceram. Int.*, 2024, **50**, 18681–18688, DOI: 10.1016/j.ceramint.2024.02.356.

39 Y. V. Baklanova, O. A. Lipina, A. N. Enyashin, L. L. Surat, A. P. Tyutyunnik, N. V. Tarakina, A. D. Fortes, A. Yu. Chufarov, E. V. Gorbatov and V. G. Zubkov, Nd^{3+},Ho^{3+}-codoped apatite-related $NaLa_9(GeO_4)_6O_2$ phosphors for the near- and middle-infrared region, *Dalton Trans.*, 2018, **47**, 14041–14051, DOI: 10.1039/C8DT02716A.

40 N. Bednarska-Adam, J. Pisarska, M. Kuwik, T. Goryczka, M. Zubko and W. A. Pisarski, Synthesis and photoluminescent characterization of ceramic phosphors Li_2MgGeO_4:Ln^{3+} (Ln^{3+} = Pr^{3+} or Tm^{3+}) under different excitation wavelengths, *RSC Adv.*, 2023, **13**, 12386, DOI: 10.1039/D3RA00500C.

41 S. Wan, S. Zhang, X. Gong, Y. Zeng, S. Jiang and J. You, Structural investigations on two typical lithium germanate melts by *in situ* Raman spectroscopy and density functional theory calculations, *CrystEngComm*, 2020, **22**, 701–707, DOI: 10.1039/C9CE01512D.

42 Z. Yang, Y. Tang, J. Li, W. Fang, J. Ma, A. Yang, L. Liu and F. Fang, Crystal structure, Raman spectra and microwave dielectric properties of novel low-temperature cofired ceramic Li_4GeO_4, *J. Alloys Compd.*, 2021, **867**, 159059, DOI: 10.1016/j.jallcom.2021.159059.

43 E. I. Kamitsos, Y. D. Yiannopoulos, M. A. Karakassides, G. D. Chryssikos and H. Jain, Raman and Infrared Structural Investigation of $xRb_2O_{(1-x)}GeO_2$ Glasses, *J. Phys. Chem.*, 1996, **100**, 11755–11765, DOI: 10.1021/jp960434+.

44 V. B. R. Boppana, N. D. Hould and R. F. Lobo, Synthesis, characterization and photocatalytic properties of novel zinc germanate nano-materials, *J. Solid State Chem.*, 2011, **184**, 1054–1062, DOI: 10.1016/j.jssc.2011.02.022.

45 B. Xu, C. Jin, J.-S. Park, H. Liu, X. Lin, J. Cui, D. Chen and J. Qiu, Emerging near-infrared luminescent materials for next-generation broadband optical communications, *InfoMat*, 2024, **6**, e12550, DOI: 10.1002/inf2.12550.

46 M. Kochanowicz, J. Żmojda, P. Miluski, A. Baranowska, K. Sadowska, M. Kuwik, J. Pisarska, W. A. Pisarski and D. Dorosz, Ultra-broadband emission in Er^{3+}/Tm^{3+}/Ho^{3+} triply-doped germanate glass and double-clad optical fiber, *Opt. Mater. Express*, 2022, **12**, 2332–2342, DOI: 10.1364/OME.462653.

47 J. Markiewicz, M. Kochanowicz, T. Ragiń, K. Sadowska, J. Żmojda, P. Miluski, J. Dorosz, M. Kuwik, W. A. Pisarski, J. Pisarska, M. Leśniak and D. Dorosz, Broadband 1.5-2.1 μm emission in gallo-germanate dual-core optical fiber co-doped with Er^{3+} and Yb^{3+}/Tm^{3+}/Ho^{3+}, *Opt. Express*, 2023, **31**, 28850–28858, DOI: 10.1364/OE.496574.

48 W. A. Pisarski, J. Pisarska, D. Dorosz and J. Dorosz, Towards lead-free oxyfluoride germanate glasses singly doped with Er^{3+} for long-lived near-infrared luminescence, *Mater. Chem. Phys.*, 2014, **148**, 485–489, DOI: 10.1016/j.matchemphys.2014.08.020.

49 J. Pisarska, M. Kuwik, A. Górny, J. Dorosz, M. Kochanowicz, J. Żmojda, M. Sitarz, D. Dorosz and W. A. Pisarski, Influence of transition metal ion concentration on near-infrared emission of Ho^{3+} in barium gallo-germanate glasses, *J. Alloys Compd.*, 2019, **793**, 107–114, DOI: 10.1016/j.jallcom.2019.04.154.

50 J. Pisarska, M. Kuwik, A. Górny, M. Kochanowicz, J. Żmojda, J. Dorosz, D. Dorosz, M. Sitarz and W. A. Pisarski, Holmium doped barium gallo-germanate glasses for near-infrared luminescence at 2000 nm, *J. Lumin.*, 2019, **215**, 116625, DOI: 10.1016/j.jlumin.2019.116625.

51 K. Kowalska, M. Kuwik, J. Pisarska, M. Leśniak, D. Dorosz, M. Kochanowicz, J. Żmojda, J. Dorosz and W. A. Pisarski, Influence of TiO_2 concentration on near-infrared luminescence of Er^{3+} ions in barium gallogermanate glasses, *J. Mater. Res. Technol.*, 2022, **21**, 4761–4772, DOI: 10.1016/j.jmrt.2022.11.081.

52 J. Pisarska, K. Kowalska, M. Kuwik, J. Dorosz, M. Kochanowicz, J. Żmojda, D. Dorosz and W. A. Pisarski, Optical properties of titanate-germanate glasses containing Ho^{3+} ions, *Mater. Res. Bull.*, 2023, **166**, 112353, DOI: 10.1016/j.materresbull.2023.112353.

53 M. Kuwik, K. Kowalska, J. Pisarska, M. Kochanowicz, J. Żmojda, J. Dorosz, D. Dorosz and W. A. Pisarski, Influence of TiO_2 concentration on near-infrared emission of germanate glasses doped with Tm^{3+} and Tm^{3+}/Ho^{3+} ions, *Ceram. Int.*, 2023, **49**, 41090–41097, DOI: 10.1016/j.ceramint.2023.03.305.

54 K. Kowalska, M. Kuwik, J. Pisarska and W. A. Pisarski, Thulium-doped titanate-germanate glasses for infrared photonics, *J. Lumin.*, 2024, **272**, 120649, DOI: 10.1016/j.jlumin.2024.120649.

55 Y. Yan, A. J. Faber and H. de Waal, Luminescence quenching by OH groups in highly Er-doped phosphate glasses, *J. Non-Cryst. Solids*, 1995, **181**, 283–290, DOI: 10.1016/S0022-3093(94)00528-1.

56 Q. Nie, L. Lu, T. Xu, S. Dai, X. Shen, X. Liang, X. Zhang and X. Zhang, Effect of hydroxyl groups on Er^{3+} doped Bi_2O_3–B_2O_3–SiO_2 glasses, *J. Phys. Chem. Solids*, 2007, **68**, 477–481, DOI: 10.1016/j.jpcs.2006.10.003.

57 S. Dai, C. Yu, G. Zhou, J. Zhang and G. Wang, Effect of OH^- content on emission properties in Er^{3+}-doped tellurite glasses, *J. Non-Cryst. Solids*, 2008, **354**, 1357–1360, DOI: 10.1016/j.jnoncrysol.2006.10.086.

58 M. Cai, Y. Lu, R. Cao, Y. Tian, S. Xu and J. Zhang, 2 μm emission properties and hydroxyl groups quenching of Tm^{3+} in germanate-tellurite glass, *Opt. Mater.*, 2016, **57**, 236–242, DOI: 10.1016/j.optmat.2016.03.055.

59 X. Fan, P. Kuan, K. Li, L. Zhang, D. Li and L. Hu, Spectroscopic properties and quenching mechanism of 2 μm emission in Ho^{3+} doped germanate glasses and fibers, *Opt. Mater. Express*, 2015, **5**, 1356–1365, DOI: 10.1364/OME.5.001356.

60 G. Gorni, R. Balda, J. Fernandez, J. J. Velazquez, L. Pascual, J. Mosa, A. Duran and Y. Castro, $80SiO_2$-$20LaF_3$ oxyfluoride glass ceramic coatings doped with Nd^{3+} for optical applications, *Int. J. Appl. Glass Sci.*, 2018, **9**, 208–217, DOI: 10.1111/ijag.12338.

61 T. Moon, S.-T. Hwang, D.-R. Jung, D. Son, C. Kim, J. Kim, M. Kang and B. Park, Hydroxyl-quenching effects on the photoluminescence properties of SnO_2:Eu^{3+} nanoparticles, *J. Phys. Chem. C*, 2007, **111**, 4164–4167, DOI: 10.1021/jp067217l.

62 L. U. Khan and Z. U. Khan, Rare Earth Luminescence: Electronic Spectroscopy and Applications, in *Handbook of Materials Characterization*, ed. K. Sharma, Springer International Publishing AG, Part of Springer Nature, 2018, ch. 10, pp. 345–404, DOI: 10.1007/978-3-319-92955-2_10.

63 F. Gennari, J. Perisa, M. Sekulic, Z. Antic, M. Dramicanin and A. Toncelli, In-band luminescence thermometry in the third biological window and multicolor emission of Er-doped fluoride and oxide nanoparticles, *J. Lumin.*, 2024, **269**, 120520, DOI: 10.1016/j.jlumin.2024.120520.

64 A. R. Pusdekar, N. S. Ugemuge, R. Nafdey and S. V. Moharil, Spectroscopic analysis of NIR emitting phosphors based on $NaLaMgWO_6$ doped with Nd^{3+} and Er^{3+}, *Spectrochim. Acta, Part A*, 2025, **330**, 125661, DOI: 10.1016/j.saa.2024.125661.

65 T. Böttger, Y. Sun, C. W. Thiel and R. L. Cone, Spectroscopy and dynamics of Er^{3+}:Y_2SiO_5 at 1.5 μm, *Phys. Rev. B: Condens. Matter Mater. Phys.*, 2006, **74**, 075107, DOI: 10.1103/PhysRevB.74.075107.

66 L. Feng, Z. Hao, Y. Luo, X. Zhang, L. Zhang, G. Pan, H. Wu and J. Zhang, Observation and photoluminescence properties of two Er^{3+} centers in $CaSc_2O_4$:Er^{3+},Yb^{3+} upconverting phosphor, *J. Alloys Compd.*, 2017, **708**, 827–833, DOI: 10.1016/j.jallcom.2017.03.088.

67 A. Enachi, O. Toma and Ş. Georgescu, Luminescent Er^{3+} centers in $CaSc_2O_4$:Er^{3+}:Yb^{3+} upconversion phosphor, *J. Lumin.*, 2021, **231**, 117816, DOI: 10.1016/j.jlumin.2020.117816.

68 S. Huang and G. Li, Photoluminescence properties of Li_2SrGeO_4:RE^{3+} (RE = Ce/Tb/Dy) phosphors and enhanced luminescence through energy transfer between Ce^{3+} and Tb^{3+}/Dy^{3+}, *Opt. Mater.*, 2014, **36**, 1555–1560, DOI: 10.1016/j.optmat.2014.04.024.

69 R. Reddappa, L. Lakshmi Devi, P. Babu, I. R. Martín, V. Lavín, V. Venkatramu, U. R. Rodríguez-Mendoza and C. K. Jayasankar, Structural, morphological and photoluminescence properties of Ca_2SiO_4:Er^{3+} phosphors synthesized from agro-food waste materials, *Ceram. Int.*, 2022, **48**, 37013–37019, DOI: 10.1016/j.ceramint.2022.08.271.

70 W. Yao, H. Chen, H. Uehara and R. Yasuhara, Spectroscopic properties of Er:BZMT ceramics for laser emission, *Opt. Mater. Express*, 2020, **10**, 3226–3234, DOI: 10.1364/OME.408858.

71 N. X. Ca, N. T. Hien, X. Fan, P. V. Do, V. H. Yen, P. V. Hao, L. K. Quynh, T. T. T. Huong and V. X. Quang, New insights on the luminescence properties and Judd–Ofelt analysis of Er-doped ZnO semiconductor quantum dots, *RSC Adv.*, 2023, **13**, 27292–27302, DOI: 10.1039/d3ra05005j.

72 R. Balda, A. Oleaga, J. Fernandez and J. M. Fdez-Navarro, Spectroscopy and frequency upconversion of Er^{3+} ions in lead niobium germanate glasses, *Opt. Mater.*, 2003, **24**, 83–90, DOI: 10.1016/S0925-3467(03)00109-5.

73 H. Yamauchi and Y. Ohishi, Spectroscopic properties of Er^{3+}-doped PbO-Ga_2O_3-GeO_2 glass for optical amplifiers, *Opt. Mater.*, 2005, **27**, 679–690, DOI: 10.1016/j.optmat.2004.04.018.

74 L. M. Marcondes, R. O. Evangelista, R. R. Goncalves, A. S. S. de Camargo, D. Manzani, M. Nalin, F. C. Cassanjes and G. Y. Poirier, Er^{3+}-doped niobium alkali germanate glasses and glass-ceramics: NIR and visible luminescence properties, *J. Non-Cryst. Solids*, 2019, **521**, 119492, DOI: 10.1016/j.jnoncrysol.2019.119492.

75 H. Zhang, T. Jia, X. Shang, S. Zhang, Z. Sun and J. Qiu, Mechanisms of the blue emission of $NaYF_4$:Tm^{3+} nanoparticles excited by an 800 nm continuous wave laser, *Phys. Chem. Chem. Phys.*, 2016, **18**, 25905–25914, DOI: 10.1039/C6CP04413A.

76 R. Fartas, M. Diaf, I. R. Martin, F. Paz-Buclatin and J. P. Jouart, Near infrared and upconversion luminescence of Tm^{3+}-Yb^{3+}codoped CdF_2 single crystals, *J. Lumin.*, 2020, **228**, 117594, DOI: 10.1016/j.jlumin.2020.117594.

77 R. Xu, L. Xu, L. Hu and J. Zhang, Structural origin and laser performance of thulium-doped germanate glasses, *J. Phys. Chem. A*, 2011, **115**, 14163–14167, DOI: 10.1021/jp207574m.

78 S. Gao, X. Liu, X. Fan, X. Li, T. Xue, K. Li, M. Liao and L. Hu, 2 μm emission properties and non-radiative processes of Tm^{3+} in germanate glass, *J. Appl. Phys.*, 2014, **116**, 173108, DOI: 10.1063/1.4900534.

79 S. Gao, X. Fan, X. Liu, M. Liao and L. Hu, Mechanical and ~2 μm emission properties of Tm^{3+}-doped GeO_2-TeO_2(or SiO_2)-PbO-CaO glasses, *Opt. Mater.*, 2015, **45**, 167–170, DOI: 10.1016/j.optmat.2015.03.028.

80 S. Nishimura, Y. Nanai, S. Koh and S. Fuchi, Luminescence properties of Tm_2O_3-doped germanate glass phosphors for near-infrared wideband light- source, *J. Mater. Sci.: Mater. Electron.*, 2021, **32**, 14813–14822, DOI: 10.1007/s10854-021-06035-w.

81 R. F. Falci, T. Guerineau, J. L. Delarosbil and Y. Messaddeq, Spectroscopic properties of gallium-rich germano-gallate glasses doped with Tm^{3+}, *J. Lumin.*, 2022, **249**, 119014, DOI: 10.1016/j.jlumin.2022.119014.

82 O. A. Lipina, Ya. V. Baklanova, L. L. Surat, M. A. Melkozerova, A. Yu. Chufarov, A. P. Tyutyunnik and V. G. Zubkov, Structural and optical characterization of Tm^{3+}-doped apatite related $NaLa_9(GeO_4)_6O_2$ phosphors, *Ceram. Int.*, 2020, **46**, 26416–26424, DOI: 10.1016/j.ceramint.2020.03.225.

83 N. A. Safronova, R. P. Yavetskiy, O. S. Kryzhanovska, M. V. Dobrotvorska, A. E. Balabanov, I. O. Vorona, A. V. Tolmachev, V. N. Baumer, I. Matolínova, D. Yu. Kosyanov, O. O. Shichalin, E. K. Papynov, S. Hau and C. Gheorghe, A novel IR-transparent Ho^{3+}:Y_2O_3-MgO nanocomposite ceramics for potential laser applications, *Ceram. Int.*, 2021, **47**, 1399–1406, DOI: 10.1016/j.ceramint.2020.08.263.

84 V. Singh, V. K. Rai, B. Voss, M. Haase, R. P. S. Chakradhar, D. T. Naidu and S. H. Kim, Photoluminescence study of nanocrystalline Y_2O_3:Ho^{3+} phosphor, *Spectrochim. Acta, Part A*, 2013, **109**, 206–212, DOI: 10.1016/j.saa.2013.01.082.

85 V. Singh and M. Seshadrib, Perovskite $SrZrO_3$:Ho^{3+} phosphors: synthesis, structure, Judd–Ofelt analysis and photoluminescence properties, *RSC Adv.*, 2023, **13**, 27782–27791, DOI: 10.1039/d3ra04175a.

86 V. Singh, A. A. Bhat, M. Radha, M. Seshadri, S. H. Nandyala and J. B. Joo, Investigation on structure and photoluminescence properties of Ho^{3+} doped $Ca_3(VO_4)_2$ phosphors for luminescent devices, *RSC Adv.*, 2024, **14**, 18777–18786, DOI: 10.1039/d4ra03178d.

87 E. Kumi-Barimah, Y. Chen, G. Sharma and A. Jha, Judd-Ofelt analysis, visible to NIR photoluminescence emission under 450 nm and 976 nm excitations and energy transfer of barium fluorotellurite glasses doping with Ho^{3+}, Yb^{3+}, Ho^{3+}:Yb^{3+}, *Opt. Mater.: X*, 2022, **16**, 100201, DOI: 10.1016/j.omx.2022.100201.

88 P. Loiko, L. Basyrova, R. Maksimov, V. Shitov, M. Baranov, F. Starecki, X. Mateos and P. Camy, Comparative study of Ho:Y_2O_3 and Ho:$Y_3Al_5O_{12}$ transparent ceramics produced from laser-ablated nanoparticles, *J. Lumin.*, 2021, **240**, 118460, DOI: 10.1016/j.jlumin.2021.118460.

89 T. Netolicky, L. Benes, K. Melanova, S. Slang, J. Oswald and T. Wagner, Near-infrared emission in Ho^{3+}-doped $Yb_3Ga_5O_{12}$ garnet nanocrystals, *J. Lumin.*, 2022, **251**, 119230, DOI: 10.1016/j.jlumin.2022.119230.

90 K. Suzuki, Absolute Photoluminescence Quantum Yield of Phosphors, in *Phosphor Handbook: Experimental Methods for Phosphor Evaluation and Characterization*, ed. R.-S. Liu and X.-J. Wang, CRS Press, 3rd edn, 2022, ch. 13, pp. 455–488, DOI: 10.1201/9781003098669.

91 Y. Li, S. Zeng and J. Hao, Non-invasive optical guided tumor metastasis/vessel imaging by using lanthanide nanoprobe with enhanced down-shifting emission beyond 1500 nm, *ACS Nano*, 2019, **13**, 248–259, DOI: 10.1021/acsnano.8b05431.

92 Y. Li, P. Zhang, H. Ning, J. Zeng, Y. Hou, L. Jing, C. Liu and M. Gao, Emitting/sensitizing ions spatially separated lanthanide nanocrystals for visualizing tumors simultaneously through up- and down-conversion near-infrared II luminescence *in vivo*, *Small*, 2019, **15**, 1905344, DOI: 10.1002/smll.201905344.

93 X. Lei, R. Li, D. Tu, X. Shang, Y. Liu, W. You, C. Sun, F. Zhang and X. Chen, Intense near-infrared-II luminescence from $NaCeF_4$:Er/Yb nanoprobes for *in vitro* bioassay and *in vivo* bioimaging, *Chem. Sci.*, 2018, **9**, 4682, DOI: 10.1039/c8sc00927a.

94 S. Liu, Z. An, J. Huang and B. Zhou, Enabling efficient NIR-II luminescence in lithium sublattice core-shell nanocrystals towards Stark sublevel based nanothermometry, *Nano Res.*, 2023, **16**, 1626–1633, DOI: 10.1007/s12274-022-5121-9.

95 E. Madirov, D. Busko, I. A. Howard, B. S. Richards and A. Turshatov, Absolute quantum yield for understanding upconversion and downshift luminescence in PbF_2:Er^{3+},Yb^{3+} crystals, *Phys. Chem. Chem. Phys.*, 2023, **25**, 11986–11997, DOI: 10.1039/d3cp00936j.

96 F. Arteaga Cardona, N. Jain, R. Popescu, D. Busko, E. Madirov, B. A. Arús, D. Gerthsen, A. De Backer, S. Bals, O. T. Bruns, A. Chmyrov, S. Van Aert, B. S. Richards and D. Hudry, Preventing cation intermixing enables 50% quantum yield in sub-15 nm short-wave infrared-emitting rare-earth based core-shell nanocrystals, *Nat. Commun.*, 2023, **14**, 4462, DOI: 10.1038/s41467-023-40031-4.